2014

Multi-variable Extremum Seeking Control for Mini-split Air-conditioning System

Yan Xiao
The University of Texas at Dallas, United States of America, yxx123430@utdallas.edu

Yaoyu Li
The University of Texas at Dallas, United States of America, yxl115230@utdallas.edu

John E. Seem
Johnson Controls Inc. , United States of America, john.seem@gmail.com

Multi-variable Extremum Seeking Control for Mini-split Air-conditioning System

Yan Xiao[1]*, Yaoyu Li[2], John E. Seem[3], Liujia Dong[4]

[1] Department of Electrical Engineering,
The University of Texas at Dallas
Dallas, TX 75080, USA
yxx123430@utdallas.edu

[2] Department of Mechanical Engineering,
The University of Texas at Dallas
Dallas, TX 75080, USA
yaoyu.li@utdallas.edu

[3] High Altitude Trading, Inc.
Jackson, WY 83001, USA
john.seem@gmail.com

[4] Department of Mechanical Engineering,
The University of Texas at Dallas
Dallas, TX 75080, USA
lxd122030@utdallas.edu

* Corresponding Author

ABSTRACT

In this study, a multi-variable extremum seeking control (ESC) scheme is proposed for a variable-speed mini-split air-conditioning system. The control inputs are the evaporator and condenser fan speeds, respectively. While the total power consumption is used as the feedback. The multi-variable ESC can optimize the control inputs for each channel in real-time, without relying on the accurate model of the system. This nearly model free feature makes the system more easily to be designed and deployed. First, the multi-variable ESC algorithm is deployed on a Dymola-based ASHP model to show its effectiveness in searching the optimal working point. Then, an experiment set-up is built to further demonstrate the promising performance in improving the efficiency of the mini-split AC system via multi-variable ESC.

1. INTRODUCTION

Ductless split air conditioning (AC) system, also known as variable refrigerant flow (VRF) system, is widely used in commercial and residential buildings (Roth et al. 2006). By eliminating the need for air duct, such system is flexible to configure, resulting cost-effective and energy saving. Mini-split ductless systems are widely adopted for residual applications. For ductless systems, with variable-speed operation of evaporator and condenser fans, as well as the variable-capacity compressor operation, such AC system can be controlled more flexibly towards better efficiency. Similar to many other air conditioning systems, model based control strategies are limited by the lack of accurate models due to the high uncertainties in the zonal cooling load and the equipment characteristics. Extremum Seeking Control (ESC) is a nearly-model free optimization method, which has received more attentions for building HVAC controls during past decades (Li Pengfei et al. 2010, Li Xiao et al. 2013). Recently, Burns and Laughman (2012), the author uses the single-input ESC to find the optimal evaporator fan speed. In this study, a multi-variable ESC

scheme is applied to find the optimal speeds for both evaporator fan and condenser fan. According to the recent development in multi-variable ESC (Ghaffari et al. 2012), the Newton-based ESC with Hessian estimation in general outperforms the Gradient-based ESC. For the gradient based ESC, the convergence speed depends on the actual Hessian, which makes the convergence speed often intractable with the unknown Hessian. Also, the off-diagonal terms of the Hessian implies coupling between different input channels, estimation of the Hessian matrix can help decouple the multi-input operation. Based on these considerations, the Newton-based ESC is adopted for this study.

2. MINI-SPLIT AC SYSTEM

A simplified diagram of a mini-split AC system is shown in Figure 1. As can be seen, there are four main components in a mini-split AC system: 1. Compressor, 2. Electronic Expansion Valve (EEV), 3. Evaporator Fan, 4. Condenser Fan. For a traditional fixed speed AC system, these four components only work in 'discrete' ON-OFF-ON-OFF manner. For variable-speed AC system, all these four components could be controlled in a 'continuous' way. This provides us the possibility of finding the optimal working point for each input, and eventually, the system's efficiency would be optimized, i.e. the power consumption is minimized. For our application, we need to override the control of evaporate fan and condenser fan speed, and use them as two control variables for our ESC controller. Figure 2 shows the control diagram of a variable speed mini-split system. The solid line represents the original control loop. While the dotted line represents the added ESC control loop.

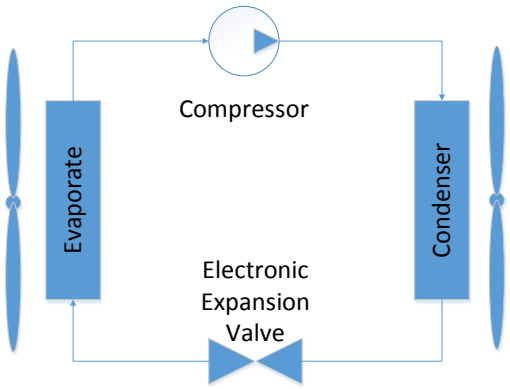

Figure 1: Diagram of a mini-split AC system

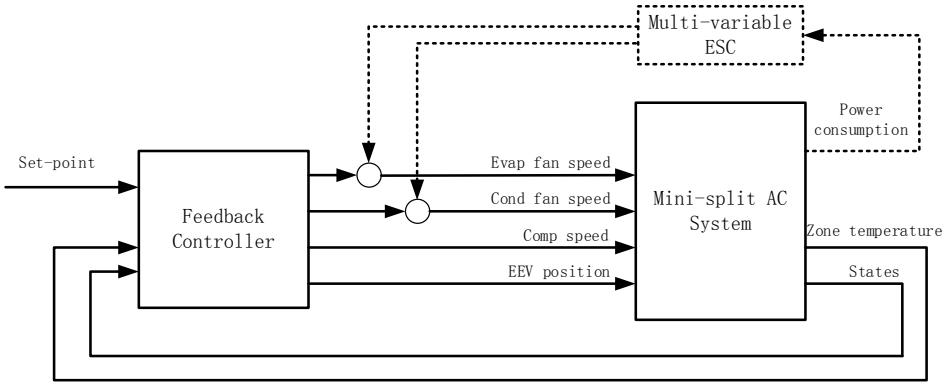

Figure 2: Control diagram of a mini-split AC system with multi-variable ESC

As can be seen, to deploy the multi-variable ESC controller is quite easy. One need simply to add a power meter to measure the power consumption of the whole mini-split AC system, and over take the speed control of evaporator fan and condenser fan. There is no need to make any other changes on the original system. With the knowledge of

the power consumption, the multi-variable ESC controller can automatically search and track the optimal speeds for both evaporator fan and condenser fan. During the searching process, the power consumption would decrease, which equals the increase in the efficiency of the mini-split AC system. In the next section, we would briefly introduce the multi-variable extremum seeking algorithm and explain why it can locate the optimal working point.

3. OVERVIEW OF MULTI-VARIABLE ESC

There are two types of multi-variable ESC schemes: 1. Gradient-based multi-variable ESC, 2. Newton-based multi-variable ESC. These two schemes are reviewed briefly as follows.

3.1 Gradient-based Multi-variable Extremum Seeking Control

Figure 3 shows the diagram of gradient-based multi-variable ESC scheme.

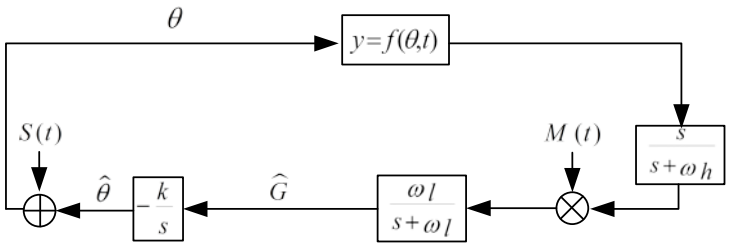

Figure 3: Diagram of gradient-based multi-variable ESC

where $S(t) = [a_1 \sin(\omega_1 t) \dots a_n \sin(\omega_n t)]^T$ is the dither signal vector added to the references of the plant, $M(t) = [\frac{2}{a_1}\sin(\omega_1 t) \dots \frac{2}{a_n}\sin(\omega_n t)]^T$ is the demodulation signal used to extract the gradient information. a_i is the dither amplitude associate with each input variable. θ is the references of the plant input, $\hat{\theta}$ is the references without dither signal. $\hat{G}$ is the estimated gradient information, $\frac{s}{s+\omega_h}$ and $\frac{\omega_l}{s+\omega_l}$ are high-pass and low-pass filter, respectively. Note that for multi-variable ($N \geq 2$) case, $S(t)$, θ, $M(t)$, $\hat{G}$, $\hat{\theta}$ are all vectors with N dimensions. By modulation and demodulation, the gradient $\hat{G}$ with reference to different control variables can be estimated. The integrator is then used to drive the gradient to zero. For a convex performance map, a point with zero gradients would mean that this point is the optimum working point.

3.2 Newton-based Multi-variable Extremum Seeking Control

Figure 4 shows the diagram of Newton-based multi-variable ESC scheme.

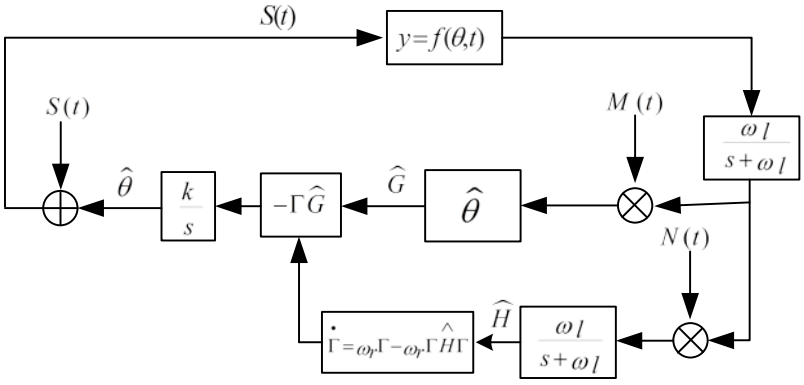

Figure 4: Diagram of Newton-based multi-variable ESC

As can be seen, the difference between Newton-based multi-variable ESC and gradient-based multi-variable ESC is that, besides gradient estimation, Newton-based multi-variable ESC also includes a Hessian estimator. By multiplying the demodulation signal $N(t)$ (for the specific mathematical expression of $N(t)$, please refer to Ghaffari et al. 2012), and filtering out the AC components, the Hessian information can be derived. Direct inversion of the estimated Hessian is not advisable since the estimated Hessian might be singular. To address this problem, a Riccati equation $\dot{\Gamma} = \omega_r \Gamma - \omega_r \Gamma \hat{H} \Gamma$ is used to derive the inversion of estimated Hessian. The purpose of utilizing Riccati equation is two folds: 1. it provides a simple way to obtain the inversion of a matrix, 2. Riccati equation works as a dynamic filter that can endure occasional ill conditioned Hessian.

For gradient-based multi-variable ESC, the convergence speed hinges on the unknown Hessian of the plant's performance map. By multiplying the estimated gradient $\hat{G}$ with inversion of estimated Hessian Γ, Newton-based multi-variable ESC eliminated the dependence on Hessian for convergence speed. This feature is especially useful for application where there exists coupling between different control variables, since this would decouple them and make the convergence speed independent for each control variable and hence more controllable for users. For our application, we plan to implement gradient-based multi-variable ESC as the first step. After that, Newton-based multi-variable ESC would be implemented and compared with the gradient-based ESC.

4. DESIGN GUIDELINE FOR MULTI-VARIABLE ESC CONTROLLER

4.1 Analysis on optimal selection of dither frequencies

For multi-variable ESC:

$$y = f[\hat{\theta} + s(t)] = f(\hat{\theta}) + g(\hat{\theta})s(t) + \frac{1}{2}s(t)^T Hs(t) + R(s(t)) \tag{1}$$

where $R(s(t))$ stands for high-order components. For the scenario where performance map resembles a quadratic function or when the input vectors is sufficiently close to the extremum point, $R(s(t))$ is considerably small and can be omitted. In the following analysis, $R(s(t))$ is ignored for simplicity. To further simplify the analysis, we use cosine to express both sine and cosine in the result. Since we are only interested in the relationship between dither frequencies, omitting the phase in each trigonometric function would have no effect on our analysis.

For a N-variable system (for multi-variable cases, $N \geq 2$), the output of the plant can be expressed as:

$$y = \sum_{i=1}^{N} f(q_i) + \sum_{i=1}^{N} g_i \cos(w_i t) + \frac{1}{2}\sum_{i=1}^{N} h_{ii}\cos(w_i t)\cos(w_i t) + \sum_{1 \leq i < j \leq N} h_{ij}\cos(w_i t)\cos(w_j t) \tag{2}$$

Note that since Hessian is symmetric, we have $h_{ij} = h_{ji}$.
The DC parts of equation (2) are:

$$\sum_{i=1}^{N} f(\theta_i), \sum_{i=1}^{N} h_{ii}$$

Note that the real value for the latter one should be $\frac{1}{4}\sum_{i=1}^{N} h_{ii}$. However, in the following analysis, we would ignore the coefficient for simplicity.
AC parts are:

$$\sum_{i=1}^{N} g_i \cos(\omega_i t) \tag{3}$$

$$\sum_{i=1}^{N} h_{ii}\cos(2\omega_i t) \tag{4}$$

$$\sum_{1 \leq i < j \leq N} h_{ij}[\cos(\omega_i + \omega_j)t + \cos(\omega_j - \omega_i)t] \tag{5}$$

After HPF, DC parts are eliminated. The remaining AC parts would be multiplied by the demodulation signal to 'extract' the Gradient and Hessian information.

To obtain the gradient g_r, where r = 1,2,…N, multiply the AC parts of Equation(2) by demodulation signal $\cos \omega_r$. Note that the Gradient information is hidden in Equation (3). After multiplication, the DC part is: g_r, which is what we intend to acquire.
Thes AC parts are:

$$g_r \cos(2\omega_r t) \tag{6}$$

$$\sum_{i=1}^{N} g_i \cos(\omega_i t)\cos(\omega_r t) = \sum_{i=1}^{N} g_i[\cos(\omega_i+\omega_r)t + \cos(\omega_i - \omega_r)t], \text{ for } \forall i \neq r \tag{7}$$

$$\sum_{i=1}^{N} h_{ii} \cos(2\omega_i t)\cos(\omega_r t) = \sum_{i=1}^{N} h_{ii}[\cos(2\omega_i + \omega_r)t + \cos(2\omega_i - \omega_r)t] \tag{8}$$

$$\begin{aligned}\sum_{1\le i<j\le N} h_{ij}[\cos(\omega_i + \omega_j)t + \cos(\omega_j - \omega_i)t]\cos(\omega_r t) = \sum_{1\le i<j\le N} h_{ij}[&\cos(\omega_i + \omega_j + \omega_r)t + \cos(\omega_i + \omega_j - \omega_r)t \\ &+ \cos(\omega_j - \omega_i + \omega_r)t + \cos(\omega_j - \omega_i - \omega_r)t]\end{aligned} \tag{9}$$

Note that to ensure equation (6)-(9) have no DC terms, dither frequencies must satisfy the following three restrictions.

1. From equation (7), $\omega_r \neq \omega_i$ for $\forall i \neq r$. i.e. any two dither frequencies cannot equal to each other. Otherwise, the estimation of g_r would be corrupted by g_i .
2. From equation (8), $\omega_r \neq 2\omega_i$. i.e. any one dither frequency cannot equal to two times of any other dither frequency. Otherwise, the estimation of g_r would be corrupted by h_{ii} .
3. From equation (9), $\omega_r \neq \omega_i + \omega_j$ for $\forall i, j \neq r$ i.e. any one dither frequency cannot equal to the sum of any other two frequencies. Otherwise, the estimation of g_r would be corrupted by h_{ij} . Note that for the case where $r = i, j$, this restriction would be degenerated into the second restriction.

From the upper analysis, it is obvious that in order to ensure accurate estimations of each channel's gradient information, these three constrains have to be respected. Note that for two-variable case, we only need to satisfy the first two constrains, since r will inevitably equals to i or j.
To obtain the Hessian h_{rr} , where r = 1, 2 … N, multiply the AC parts of equation (2) by demodulation signal:

$$\cos(\omega_r t)\cos(\omega_r t) = \frac{1}{2}[\cos(2\omega_r t) + 1]$$

Note that, same as previous, we suppress the use of coefficient to simplify the procedure of analyzing. i.e. The demodulation signal is:

$$\cos(2\omega_r t) + 1 \tag{10}$$

Note that the Hessian information h_{rr} is contained in equation (4). After multiplication, the DC part is h_{rr} , which is what we are trying to derive. For the AC parts, since there is a DC component in the demodulation signal (see equation (10)), the AC parts expressed by equation (3)-(5) would be included. Besides these, the following equations are also presented in the AC signal after demodulation:

$$\sum_{i=1}^{N} g_i \cos(\omega_i t)\cos(2\omega_r t) = \sum_{i=1}^{N} g_i[\cos(\omega_i+2\omega_r)t + \cos(\omega_i - 2\omega_r)t] \tag{11}$$

$$h_{rr} \cos(4\omega_r t) \tag{12}$$

$$\sum_{i=1}^{N} h_{ii} \cos(2\omega_i t)\cos(2\omega_r t) = \sum_{i=1}^{N} h_{ii}[\cos 2(\omega_i + \omega_r)t + \cos 2(\omega_i - \omega_r)t] \text{ for } \forall i \neq r \tag{13}$$

$$\begin{aligned}\sum_{1\le i<j\le N} h_{ij}[\cos(\omega_i + \omega_j)t + \cos(\omega_j - \omega_i)t]\cos(2\omega_r t) = \sum_{1\le i<j\le N} h_{ij}[&\cos(\omega_i + \omega_j + 2\omega_r)t + \cos(\omega_i + \omega_j - 2\omega_r)t \\ &+ \cos(\omega_j - \omega_i + 2\omega_r)t + \cos(\omega_j - \omega_i - 2\omega_r)t]\end{aligned} \tag{14}$$

To ensure the estimated Hessian h_{rr} is accurate, the following constrains need to be satisfied.

4. From equation (13), $\omega_r \neq \omega_i$ for $\forall i \neq r$. i.e. any two dither frequencies cannot equal to each other. Otherwise, the estimation of h_{rr} would be corrupted by h_{ii} .
5. From equation (11), $\omega_r \neq 2\omega_i$. i.e. any one dither frequency cannot equal to two times of any other dither frequency. Otherwise, the estimation of h_{rr} would be corrupted by g_i .
6. From equation (14), $\omega_r \neq \frac{1}{2}(\omega_j \pm \omega_i)$ for $\forall i, j \neq r$ i.e. any one dither frequency cannot equal to the sum or difference of any other two frequencies divided by 2. Otherwise, the estimation of h_{rr} would be corrupted by h_{ij} . Note that for the case where $r = i, j$, this restriction would be expressed as $\omega_r \neq \omega_i$, which is the same as restriction 4. Also, $\omega_r \neq 3\omega_i$. i.e. any dither frequency cannot equal to any other dither frequency timed by three.

Finally, To obtain the Hessian h_{kl} , where $1 \leq k < l \leq N$, multiply the AC parts of equation (2) by demodulation signal:

$$\cos(\omega_k + \omega_l)t + \cos(\omega_l - \omega_k)t \tag{15}$$

Note that the Hessian information h_{kl} is contained in equation (5). After multiplication, the DC part is h_{kl} , which is what we are trying to obtain.

The AC parts are:

$$\sum_{i=1}^{N} g_i \cos(\omega_i t)\cos(\omega_k + \omega_l)t = \sum_{i=1}^{N} g_i[\cos(\omega_i+\omega_k+\omega_l)t + \cos(\omega_k + \omega_l - \omega_i)t] \tag{16}$$

$$\sum_{i=1}^{N} g_i \cos(\omega_i t)\cos(\omega_l - \omega_k)t = \sum_{i=1}^{N} g_i[\cos(\omega_i+\omega_l-\omega_k)t + \cos(\omega_l - \omega_k - \omega_i)t] \tag{17}$$

$$\sum_{i=1}^{N} h_{ii} \cos(2\omega_i t)\cos(\omega_k + \omega_l)t = \sum_{i=1}^{N} h_{ii}[\cos(2\omega_i + \omega_k + \omega_l)t + \cos(\omega_k + \omega_l - 2\omega_i)t] \tag{18}$$

$$\sum_{i=1}^{N} h_{ii} \cos(2\omega_i t)\cos(\omega_l - \omega_k)t = \sum_{i=1}^{N} h_{ii}[\cos(2\omega_i + \omega_l - \omega_k)t + \cos(\omega_l - \omega_k - 2\omega_i)t] \tag{19}$$

For the situation where i=k and j=l

$$h_{ij}[\cos 2(\omega_i + \omega_j)t + \cos(2\omega_j t) + \cos(2\omega_i t)] \tag{20}$$

For any other situation but $i=k$ and $j=l$

$$\sum_{1\leq i<j\leq N} h_{ij}[\cos(\omega_i + \omega_j)t + \cos(\omega_j - \omega_i)t]\cos(\omega_k + \omega_l)t = \sum_{1\leq i<j\leq N} h_{ij}[\cos(\omega_i + \omega_j + \omega_k + \omega_l)t + \cos(\omega_i + \omega_j - \omega_k - \omega_l)t + \cos(\omega_j - \omega_i + \omega_k + \omega_l)t + \cos(\omega_j - \omega_i - \omega_k - \omega_l)t] \tag{21}$$

$$\sum_{1\leq i<j\leq N} h_{ij}[\cos(\omega_i + \omega_j)t + \cos(\omega_j - \omega_i)t]\cos(\omega_l - \omega_k)t = \sum_{1\leq i<j\leq N} h_{ij}[\cos(\omega_i + \omega_j + \omega_l - \omega_k)t + \cos(\omega_i + \omega_j - \omega_l + \omega_k)t + \cos(\omega_j - \omega_i + \omega_l - \omega_k)t + \cos(\omega_j - \omega_i - \omega_l + \omega_k)t] \tag{22}$$

To ensure the estimated Hessian h_{kl} is accurate, the following constrains need to be satisfied.

7. From equation (16),(17), $\omega_i \neq \omega_{k+}\omega_l$ for $\forall i \neq k, l$. i.e. any dither frequency cannot equal to the sum of any other dither frequencies. For the case where $i = k \text{ or } l$, this restriction is degenerated into constraint 5. These constraints need to be satisfied. Otherwise, the estimation of h_{kl} would be corrupted by g_i .
8. Since equation (18),(19) are essentially the same as equation (14). They give the same constraint as restriction 6. Failing to obey this constraint, the estimation of h_{kl} would be corrupted by h_{ii} .
9. From equation (21),(22), $\omega_i \neq \omega_j + \omega_k \pm \omega_l$ for all distinct *i,j,k,l.* For the case where *j=k,* the constraint is degenerated into constraints 4 and 6.

To sum up: Based on the previous analysis, in order to obtain accurate estimations of the Gradient information, the dither frequencies need to satisfy:

For distinct *r,i,j*

1. $\omega_r \neq \omega_i$
2. $\omega_r \neq 2\omega_i$
3. $\omega_r \neq \omega_i + \omega_j$ (Only valid for $N \geq 3$ case)

To obtain the Hessian information, the frequency selection should further obey the following constraints:

4. $\omega_r \neq 3\omega_i$
5. $\omega_r \neq \frac{1}{2}(\omega_j \pm \omega_i)$ (Only valid for $N \geq 3$ case)
6. For distinct *i,j,k,l*, $\omega_i \neq \omega_j + \omega_k \pm \omega_l$ (Only valid for $N \geq 4$ case)

These constraints define all the feasible choice of dither frequencies. An interesting question arises here: Is there an optimal selection of the dither frequencies? To answer this question, we use a two-variable case as an example to illustrate the point of optimal dither frequency.

Assume that the upper bound frequency for the two control variable is ω_{u1} and ω_{u2} respectively (Note that the upper bound frequency for each control variable is obtained from plant's dynamics estimation). Assuming that $\omega_{u1} \leq \omega_{u2}$, then it is also reasonable to assume $\omega_1 < \omega_2$. Based on the restrictions analyzed above, the candidates for the AC components with minimum frequency are:

$$\{\omega_1, (\omega_2 - \omega_1), |\omega_2 - 2\omega_1|, |\omega_2 - 3\omega_1|\} \tag{23}$$

Then by solving the following non-linear optimal problem, we can obtain the optimal selection for dither frequencies.

$$\text{Maximize: } \min\{\omega_1, (\omega_2 - \omega_1), |\omega_2 - 2\omega_1|, |\omega_2 - 3\omega_1|\}$$

$$\text{Subject to: } \omega_1 < \omega_{u1}$$

$$\omega_2 < \omega_{u2}$$

$$0 < \omega_1 < \omega_2$$

Note that this problem is for Newton-based ESC with Hessian estimation. For gradient-based ESC where we are not concern of Hessian, the last candidates in equation (23) can be ignored.

4.2 Design guideline for multi-variable ESC

Multi-variable ESC is quite easy to be deployed. One reason is that it has only a few parameters that need to be tuned. However, fail to choose these parameters in an appropriate way would result in compromised performance, even failure. In this section, a general guide line of the parameter selection would be given.

1. **Dither Signal Amplitude:** The principle to choose the dither signal amplitude is that the amplitude should be large enough so that it can cause apparent change in the output of the plant. However, it should not be unnecessarily too large since this would result in unnecessarily large oscillation in the output. Which would compromise system's performance
2. **Dither Signal Frequency:** The principle to choose the dither signal frequencies is that it should be slower than the inherent dynamic of the plant. In another word, generally, a plant with dynamics can be seen as a low pass filter, the frequency of each dither signal should be chosen such that it is smaller than the cut-off frequency of the equivalent LPF of the plant. For multi-variable ESC case, the dither frequencies should further satisfy those six constraints given in the last section. And there exists a optimal selection such that the smallest frequencies in the AC components can be maximized. In this case, the cut-off frequency of the LPF can be optimized, which would result in a fastest convergence speed.

3. **Low Pass Filter & High Pass Filter:** The cut-off frequency of the LPF and HPF of the ESC controller should be chosen smaller than the dither frequencies.

5. SIMULATION STUDY

In this section, the multi-variable ESC algorithm is deployed to a Dymola-based Air Source Heat Pump (ASHP) model to testify its effectiveness in searching the optimal working point. First, it is important to acquire the static map of the ASHP model. Note that the static map is obtained on the premise that the heat load and the indoor temperature are constant. In another word, the cooling power is constant.

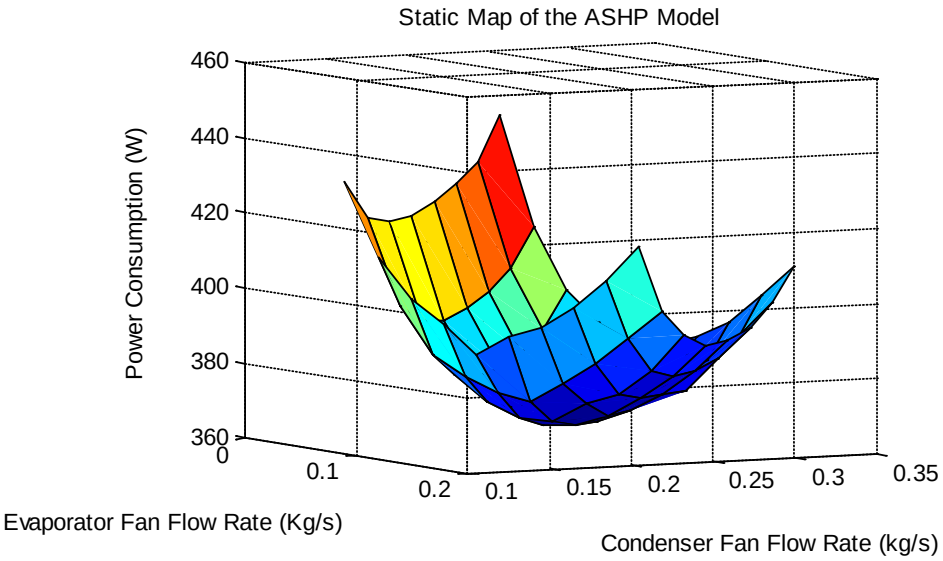

Figure 5: Static map of the ASHP model

From the static map shown above, it is obvious that the power consumption is related to both the evaporator fan speed and the condenser fan speed. And there exists a unique working point where the power consumption is minimized. This unique working point is called optimal working point. At this optimal working point, the evaporator fan flow rate is at around 0.12 kg/s. And the condenser fan flow rate is at around 0.22 kg/s. The minimum power consumption is around 366 watts.

Next, a multiple-variable ESC controller is deployed to see if it can locate the optimal working point. The simulation results are shown in **Figure 6** to **Figure 8**. Note that the ESC controller is engaged at 20,000 second.

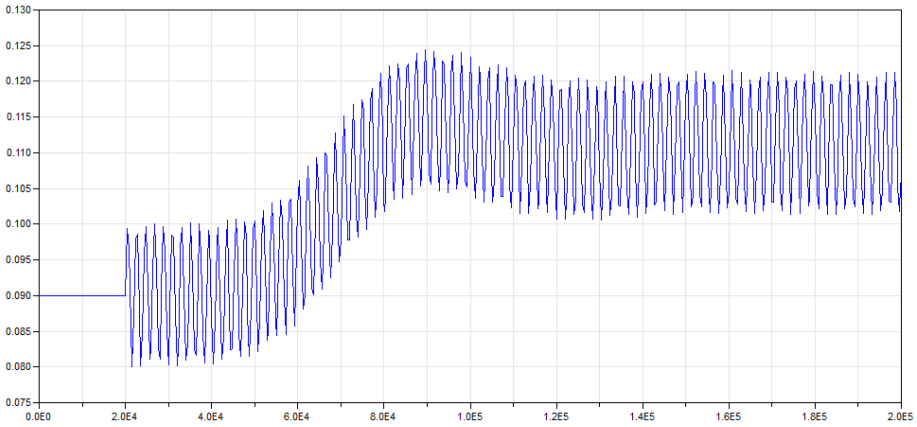

Figure 6: Evaporator fan flow rate (Abscissa: Sec, Coordinate: kg/s)

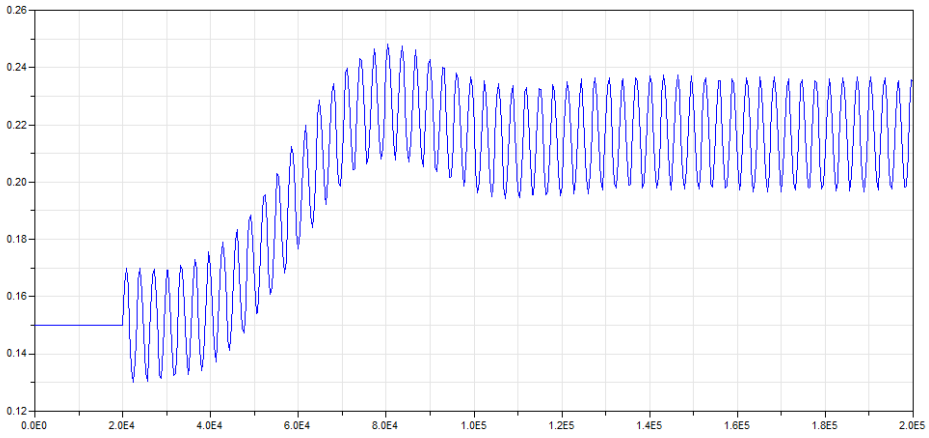

Figure 7: Condenser fan flow rate (Abscissa: Sec, Coordinate: kg/s)

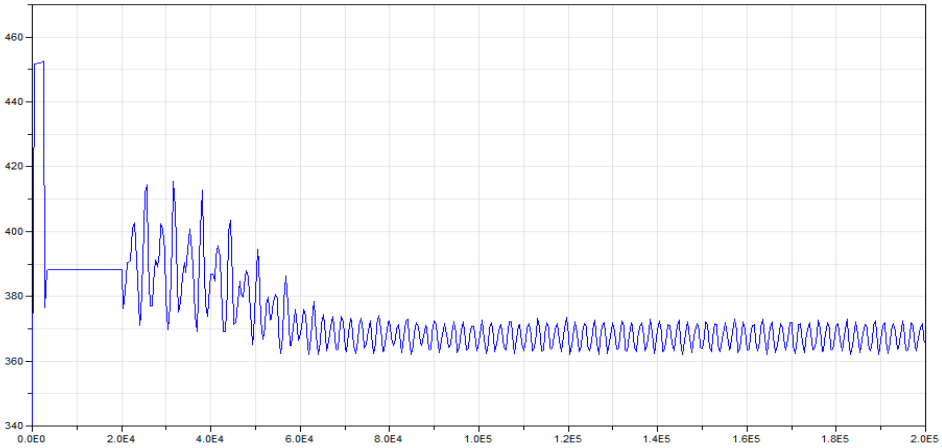

Figure 8: Power consumption (Abscissa: Sec, Coordinate: Watt)

The dither frequency for the evaporator fan is set at 0.003 rad/s. The dither frequency for the condenser fan is set at 0.002 rad/s. The dither amplitudes for the evaporator fan and condenser fan are 0.01 kg/s and 0.02 kg/s respectively. The cut-off frequencies for both the LPF and the HPF are set at 0.0002 rad/s.

The initial flow rates for the evaporator and condenser fan are set at 0.09 kg/s and 0.15 kg/s respectively. From Figure 8, we can see that after the transit, the power consumption is at around 390 watts. At 20,000 sec, the multi-variable ESC controller is engaged. After 40,000 seconds, the power consumption dropped to around 366 watts, which is the ideal minimum point. The simulation results demonstrate the effectiveness of multi-variable ESC in searching the optimal working point of an ASHP, without knowledge of the mathematic model of the ASHP.

6. EXPERIMENTAL STUDY

To further verify the effectiveness of multi-variable ESC in the application of mini-split AC system, an experiment setup is built with a 9000 BTU variable-speed mini-split AC system (Mitsubishi MSZ-GE09NA and MUY-GE09NA). A 2000 Watts electrical heater works as the heat load. The heater and the indoor unit of the mini-split system are installed in a 4’x8’x6’ insulated chamber.

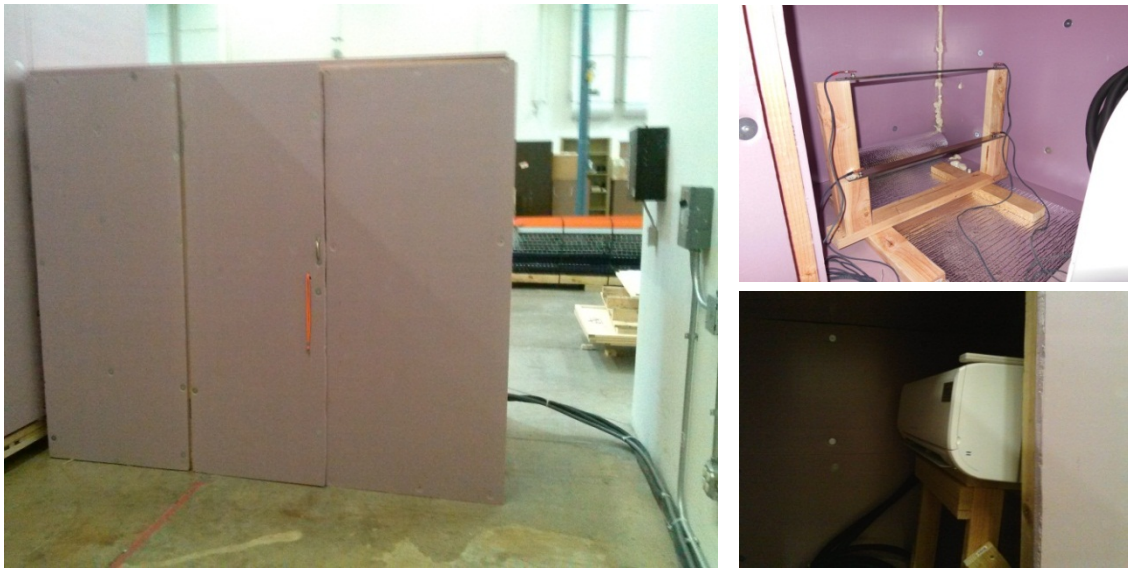

Figure 9: Pictures of experimental setup

For this study, as mentioned earlier, the objective is to implement two-variable ESC for the mini-split system. One variable is the speed of the indoor unit fan (or evaporator fan), the other variable being the speed of the outdoor unit fan, i.e. condenser fan. Note that we only override the speed control of the evaporate fan and condenser fan, all the other components (compressor, EEV etc.) are controlled with its original control logic. To achieve the speed control for the indoor unit fan, the fan speed control of the indoor unit system is customized. To achieve the speed control of the outdoor unit fan motor, a TMS320F28035 based motor control developer kit is used. A power meter (Watt Node Pulse WNB-3D-240-P) is connected to measure the power consumption of the mini-split system in real time. The ESC controller uses the measured power consumption as feedback and drive the inputs (indoor & outdoor fan speeds) to their individual optimal working point, so that the power consumption could be dropped to the lowest level, i.e. the efficiency of the mini-split system with regard to the indoor and outdoor unit fan speeds could be maximized.

The data acquisition and control algorithms are implemented on a National Instruments CompactRIO platform. During the operation, the CompactRIO reads the power consumption information sent from the power meter, which will be fed into the ESC control algorithm to get the speed reference for both the evaporator fan and condenser fan. Then, the speed references will be applied to the two motors. Meanwhile, the speed feedback for both of the motors and indoor temperature, are all monitored by the CompactRIO in real time. The speed sensor for the outdoor unit fan is OMEGA HHT13. The temperature sensor is OMEGA P-L-1/10-1/8-6-0-T-3.

For the experiments performed, the heat load is set to be 2000 W, the chamber temperature set-point is set to be 20°C (68°F), the outdoor temperature fluctuates between 27 to 28°C (80.6-82.4°F).

The parameters for the multi-variable ESC controller are chosen based on the design guidelines reviewed in Section 4.2. The dither amplitude for the evaporator fan speed is 45 rpm, the dither frequency for the evaporator fan speed control is $5.3 \times 10^{-4}\ Hz$ ($dither\ period\ T = 1870\ sec$). The dither amplitude for the condenser fan speed is 45 rpm, the dither frequency for the condenser fan speed is $7.6 \times 10^{-4}\ Hz$($dither\ period\ T = 1310\ sec$). The cut-off frequencies for both the low-pass and high-pass filters are chosen as $5 \times 10^{-4}\ Hz$. The integrator gain for both the control variables is 0.0008.

The initial fan speed for the evaporator fan is set at 700 RPM. The initial condenser fan speed is set at 250 RPM. At 1200 sec, the ESC controller is engaged. The following figures show the experimental results. The duration of the experiment is 7600 seconds.

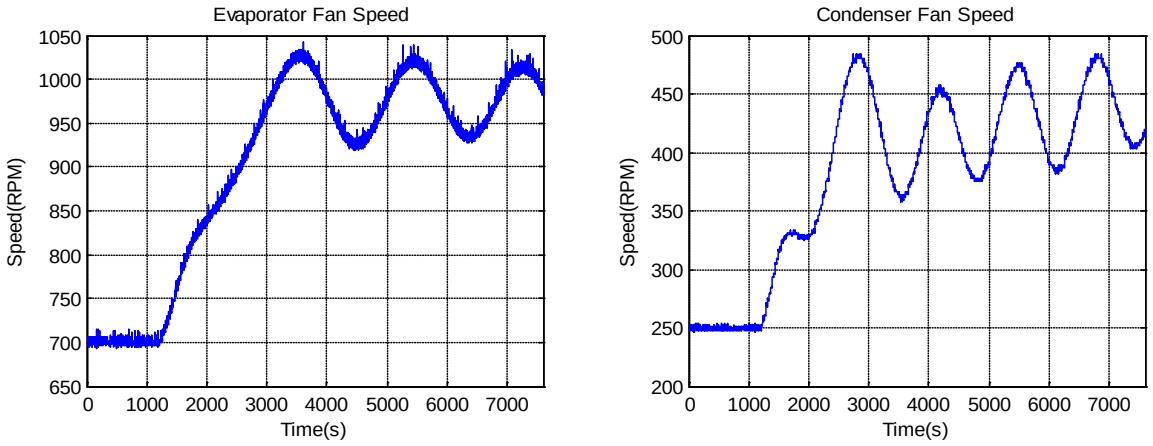

Figure 10: Evaporator and condenser fan speed

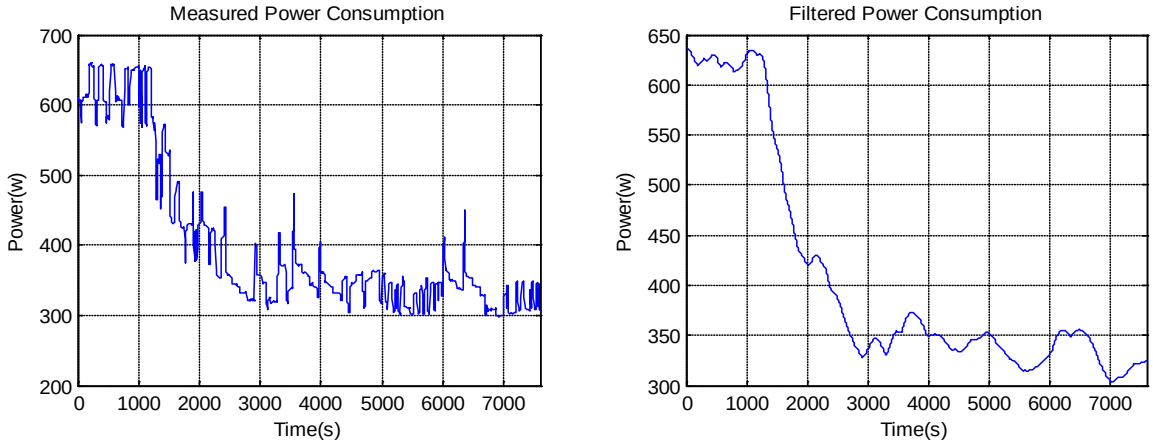

Figure 11: Measured power consumption and filtered power

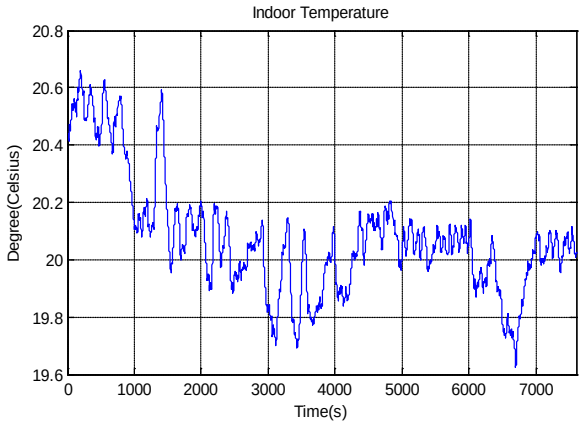

Figure 12: Indoor temperature

From Figures 10 through 12, it is seen before ESC is engaged, the power consumption with initial fan speeds (700 rpm for evaporator fan & 250 rpm for condenser fan) to maintain the set-point of the indoor temperature is around 625 W. After ESC is engaged, the evaporate fan speed is driven up to around 975 rpm, and the condenser fan speed is driven up to about 450 rpm. The power consumption is dropped to around 325W. The optimum point searching

process takes about 1800 seconds. During the experiment process, the indoor temperature is always around 20 °C, which is the temperature set-point.

7. CONCLUSIONS

This paper presents an implementation of multi-variable ESC in optimizing the working points for the evaporator and condenser fan speeds. Both simulation and experimental results show promising performance of this algorithm. Compared with model based optimization method, multi-variable ESC provides a much simpler and effective way to locate and track the optimal working points for a complicate system which is very difficult and costly to build an accurate model. Admittedly, the parameter of the experiment still needs to be improved in the future work so that the convergence speed could be faster, and the oscillation of the power consumption could be smaller.

REFERENCES

[1]. Ariyur, K. B., Krstić, M., *Real-Time Optimization by Extremum-Seeking Contro*l, John Wiley & Sons, Hoboken, NJ,2003.
[2]. Ariyur, K.B., & Krstić, M. Analysis and design of multivariable extremum seeking. In Proc. of the American control conference. 2012
[3]. Ariyur, K.B., & Krstić, M. Multivariable extremum seeking feedback: analysis and design. In Proc. of the American control conference. 2012
[4]. Burns D.J., Laughman C., "Extremum seeking control for energy optimization of vapor compression systems", International Refrigeration and Air Conditioning Conference at Purdue, pp. 2192, July 2012.
[5]. Ghaffari A., Krstić, M., Multi-variable Newton-based extremum seeking, Automatica, vol.48, pp. 1759-1767, 2012.
[6]. Ghaffari A., Krstić, M., and Seshagiri S., "Power optimization for photovoltaic micro-converters using multivariable newton-based extremum-seeking", 51st IEEE Conference on Decision and Control, Maui, Hawaii, December, 2012
[7]. Ghaffari A., Krstić, M., and Seshagiri S., "Power optimization for photovoltaic micro-converters using multivariable gradient-based extremum-seeking", 51st IEEE Conference on Decision and Control, Maui, Hawaii, December, 2012
[8]. Krstić, M. "Performance Improvement and Limitations in Extremum Seeking Control." Systems & Control Letters, 39(5):313–326, 2000.
[9]. Rotea, A. Mario, Analysis of multivariable extremum seeking algorithms, Proceedings of the American Control Conference, Chicago, Illinois, June 2000
[10]. Roth, K., Westphalen, D. and Brodrick, J. "Ductless Split Systems,"ASHRAE Journal, Vol. 48, 2006, pp. 115-117.
[11]. Neˇsi´c D., Tan Y., Moase W. and Manzie C., "A unifying approach to extremum seeking: adaptive schemes based on estimation of derivatives", 49th IEEE Conference on Decision and Control, Atlanta, GA, Dec. 2010
[12]. Moase H.W., Manzie C., Brear J.M., "Newton-like extremum-seeking for the control of themoacoustic instability", IEEE TRASACTIONS ON AUTOMATIC CONTROL, vol.55, pp.2094-2105, September 2010.
[13]. Li,P., Y. Li and J.E. Seem. 2010. Efficient Operation of Air-side Economizer Using Extremum Seeking Control. ASME Journal of Dynamic Systems, Measurement, and Control, 132(3): 031009 (10 pages)
[14]. Li, X., Y. Li, J.E. Seem. 2013. Dynamic Modeling and Self-optimizing Operation of Chilled Water Systems Using Extremum Seeking Control. Energy and Buildings, 58: 172-182.
[15]. Li,P., Y. Li and J.E. Seem. 2010. Efficient Operation of Air-side Economizer Using Extremum Seeking Control. ASME Journal of Dynamic Systems, Measurement, and Control, 132(3): 031009 (10 pages)
[16]. Li, X., Y. Li, J.E. Seem. 2013. Dynamic Modeling and Self-optimizing Operation of Chilled Water Systems Using Extremum Seeking Control. Energy and Buildings, 58: 172-182.
[17]. Mu, B., Y. Li, J.E. Seem. 2013. Comparison of Several Self-Optimizing Control Methods for Efficient Operation for a Chilled Water Plant. ASME 2013 Dynamic Systems and Control Conference, 4097, V002T25A006 (9 pages)

ACKNOWLEDGEMENTS

This work is financially supported by Building Efficiency Research Group of Johnson Controls, Inc. The authors are grateful of Dr. John House and Dr. Timothy Salsbury for their inputs and suggestions to this work.